

连接温度对 TiAl/Ti₃AlC₂ 扩散焊接头界面结构及性能的影响

宋晓国^{1,2}, 王美荣², 林兴涛¹, 刘甲坤¹, 曹 健^{1,2}, 冯吉才^{1,2}

(1. 哈尔滨工业大学 先进焊接与连接国家重点实验室, 哈尔滨 150001;

2. 哈尔滨工业大学(威海) 山东省特种焊接技术重点实验室, 威海 264209)

摘 要: 采用 Ti/Ni 复合中间层实现了 TiAl 合金和 Ti₃AlC₂ 陶瓷的扩散连接. 利用 SEM、XRD 等分析方法对接头界面结构进行了分析. 结果表明, TiAl/Ti₃AlC₂ 接头典型界面结构为 TiAl/Ti₃Al + Al₃NiTi₂/Ti₃Al/α-Ti + Ti₂Ni/Ti₂Ni/TiNi/Ni₃Ti/Ni/Ni₃(TiAl)/Ni₃Al + TiC_x + Ti₃AlC₂/Ti₃AlC₂. 随着连接温度的升高, TiAl/Ti 界面处的 Ti₃ 层逐渐减小, Ti₃Al 化合物层逐渐变厚; TiNi 化合物层厚度显著增加, Ti₂Ni 和 Ni₃Ti 层厚度基本保持不变. 接头抗剪强度随连接温度升高先增加后减小, 当连接温度为 850 °C 时, 接头的抗剪强度最高可达到 85.3 MPa. 接头主要在 Ni/Ti₃AlC₂ 界面及 Ti₃AlC₂ 基体处发生断裂.

关键词: 钛铝合金; 陶瓷; 扩散连接; 界面组织

中图分类号: TG 456.9 **文献标识码:** A **文章编号:** 0253-360X(2014)10-0009-04

0 序 言

Ti₃AlC₂ 陶瓷是一类新型的三元层状材料^[1], 具有金属和陶瓷的双重优异性能, 不仅拥有高屈服强度、高热稳定性、高弹性模量、高熔点和良好的抗氧化性能, 而且具有良好的导热和导电性, 能像金属一样进行机械加工^[2]. 另外 Ti₃AlC₂ 陶瓷特有的层状结构使其具有良好的自润滑性和较低的摩擦系数^[3]. 它既是高温发动机的理想候选材料, 同时由于其能够吸收机械震动, 并仍可以保持硬度和轻型的特点, 可以用于汽车、飞机发动机部件的制造以及精密机械工具的生产, 有望在不久的将来获得广泛应用^[4].

TiAl 合金是一种轻质高温结构材料, 以其高的比强度、比刚度, 良好的抗氧化性及优异的高温力学性能在航天领域有广泛的应用前景^[5], 尤其非常适合制造发动机中的运动部件, 在高温领域将是代替钛基合金和镍基合金的一种很有潜力的材料.

实现 TiAl 合金/Ti₃AlC₂ 陶瓷的可靠连接对于推动二者在航天及航空发动机领域的应用有着重要的

意义^[6,7]. 文中采用 Ti/Ni 复合中间层实现了 TiAl 合金与 Ti₃AlC₂ 陶瓷的扩散连接, 重点分析了连接温度对接头界面结构及力学性能的影响.

1 试验方法

试验采用的 TiAl 合金为 Ti-46Al-2Nb-2Cr, 其微观形貌如图 1 所示, 为典型的全层片组织. Ti₃AlC₂ 陶瓷由哈尔滨工业大学特种陶瓷研究所提供. 图 2 所示为其微观组织形貌, 由图 2 可见陶瓷层片状晶粒尺寸为 10 μm 左右.

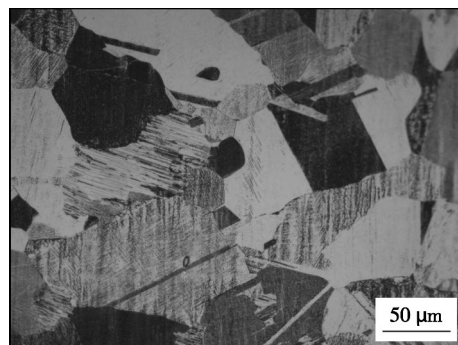


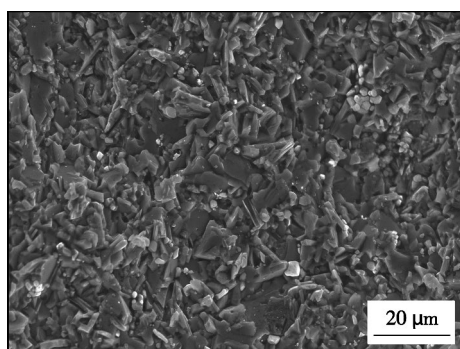
图 1 TiAl 合金显微组织形貌

Fig. 1 Microstructure of TiAl alloy

连接前采用金刚石内圆切割机将 Ti₃AlC₂ 陶瓷

收稿日期: 2014-01-10

基金项目: 国家重点基础研究发展计划资助项目(973 计划 2011CB-605505); 中国博士后科学基金资助项目(2013M531032); 浙江省钎焊材料与技术省级重点实验室开放基金资助项目

图 2 Ti_3AlC_2 陶瓷组织形貌Fig. 2 Microstructure of Ti_3AlC_2 ceramic

切成 $4\text{ mm} \times 4\text{ mm} \times 3\text{ mm}$ 大小的试样, 用线切割将 TiAl 合金切割成 $20\text{ mm} \times 10\text{ mm} \times 2\text{ mm}$ 大小的试样, 连接面积为 $4\text{ mm} \times 4\text{ mm}$, 将连接面依次用 80 号 ~ 1 500 号水砂纸逐次打磨. 中间层材料所采用钛箔厚度为 $100\text{ }\mu\text{m}$, 镍箔厚度为 $50\text{ }\mu\text{m}$. 将打磨后的试样和中间层材料放入丙酮中超声清洗 10 min 后取出晾干. 然后按照 TiAl/Ti/Ni/ Ti_3AlC_2 顺序装配并置于真空扩散炉中. 连接温度为 $750 \sim 875\text{ }^\circ\text{C}$, 保温时间为 60 min, 连接压力为 30 MPa. 采用 Instron1186 型万能试验机测试连接接头的室温抗剪强度. 利用扫描电镜和能谱仪对接头界面组织和断口形貌进行观察和分析, 并采用 X 射线衍射仪对接界面物相进行标定, 分析界面组织对接头力学性能的影响.

2 试验结果与讨论

2.1 接头典型界面组织的影响

图 3 所示为连接温度 $850\text{ }^\circ\text{C}$, 保温时间 60 min, 连接压力 30 MPa 条件下, 获得的接头典型界面组织形貌. 由图 3 可见, 在 TiAl/Ti 界面处产生了两层扩散反应层 A 和 B. 其中 A 层为黑色的基体上分布着垂直于焊缝的白色针状相, 厚度 $2\text{ }\mu\text{m}$ 左右; 位于钛箔和 A 层之间的 B 层的厚度为 $3\text{ }\mu\text{m}$ 左右, 其衬度较黑. 从 C 层上可以看到, 大量白色的蠕虫状组织均匀分布在钛箔上. 由图 3c 可以看到, 钛箔和镍箔之间生成了 D、E 和 F 三层扩散反应层, 从 D 层到 F 层, 扩散层的衬度逐渐变白. D 层和 E 层之间有一层过渡层, 跟 D 层衬度相似的灰色针状、颗粒相镶嵌在和 E 层衬度类似的浅灰色基体相中. 由图 3d 中可以明显看到镍箔和 Ti_3AlC_2 陶瓷的原始界面. 在镍箔侧形成了平均厚度为 $2.5\text{ }\mu\text{m}$ 左右的浅灰色扩散层 H. 在靠近焊缝的陶瓷上, 形成了 $10\text{ }\mu\text{m}$ 左右的陶瓷交互层 J, 这一层的反应较为剧烈, 颜色衬度和 Ti_3AlC_2 母材存在较大的差异. 在靠近 J 层的

Ti_3AlC_2 陶瓷母材上, 由于陶瓷晶粒的晶界处分布着白色相, 可以清晰看到层片状 Ti_3AlC_2 陶瓷的晶粒, 由此可以推测, 镍优先沿着 Ti_3AlC_2 陶瓷的晶界处扩散, 进而与 Ti_3AlC_2 陶瓷发生反应. 为进一步分析接头的物相, 对焊后的试样进行逐层打磨, 并对 C 层和 J 层进行了 XRD 分析, 结果分别如图 4 和图 5 所示. 结合表 1 中所示各点 EDS 成分分析结果可知, 钛箔中白色的蠕虫状组织为 Ti_2Ni 相. 在高温下 $\alpha\text{-Ti}$ 转变为 $\beta\text{-Ti}$, $\beta\text{-Ti}$ 中固溶较多的镍, 在冷却过程中, 镍就会过饱和析出, 形成 Ti_2Ni 均匀分布在钛箔上. 而陶瓷侧由于镍大量扩散进入, 并与 Ti_3AlC_2 陶瓷发生反应, 促使陶瓷分解形成 TiC_x , 且陶瓷中 Al 元素与镍结合生成了 Ni_3Al .

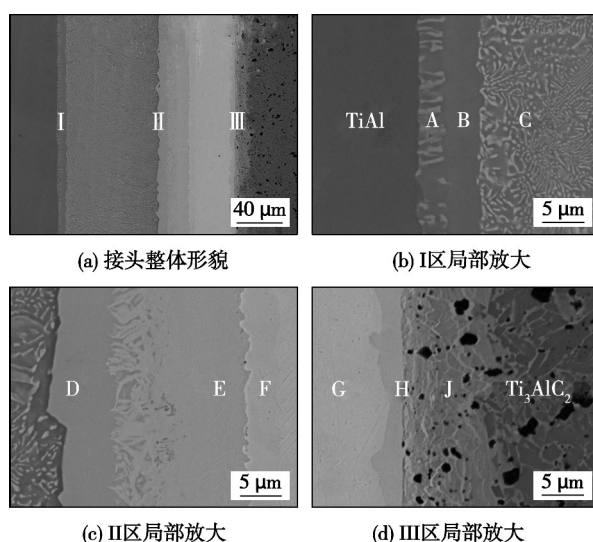
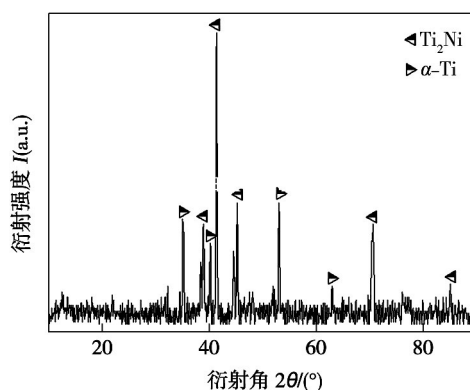
图 3 TiAl/Ti/Ni/ Ti_3AlC_2 接头典型界面结构Fig. 3 Typical interfacial microstructure of TiAl/Ti/Ni/ Ti_3AlC_2 joint

图 4 C 层 XRD 衍射结果

Fig. 4 XRD result of layer C

2.2 连接温度对接头力学性能的影响

图 6 为保温时间 60 min, 连接压力 30 MPa, 不同

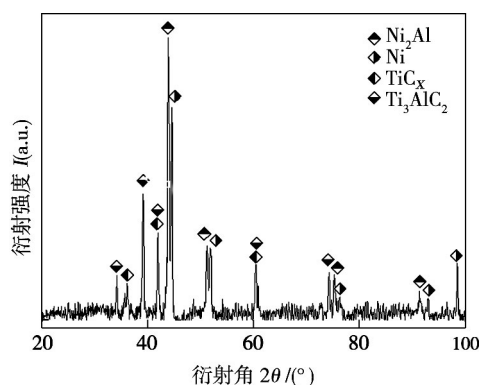


图 5 J 层 XRD 衍射结果

Fig. 5 XRD result of layer J

表 1 图 3 中各层特征点的能谱分析(原子分数, %)

Table 1 EDS results of each layer in Fig. 3

层	Ti	Al	Ni	Nb	Cr	C	可能相
A	50.50	39.19	7.61	1.88	1.29	—	Al ₃ NiTi ₂ + Ti ₃ Al
B	70.75	26.70	0.59	1.28	0.69	—	Ti ₃ Al
C	71.29	7.49	20.20	0.28	0.74	—	Ti ₂ Ni + Ti _{ss}
D	64.16	2.76	32.49	0.23	0.36	—	Ti ₂ Ni
E	47.60	1.60	50.19	0.43	0.18	—	TiNi
F	24.18	1.57	74.24	—	—	—	Ni ₃ Ti
G	1.62	0.63	97.75	—	—	—	Ni
H	5.74	21.27	72.99	—	—	—	Ni ₃ (Ti, Al)
J	36.12	18.71	26.20	—	—	18.97	TiCx + Ti ₃ AlC ₂

温度条件下 TiAl/Ti/Ni/Ti₃AlC₂ 接头的组织形貌。当温度在 750 ~ 850 °C 时,随着温度的改变,界面结构变化不大,各个反应层的厚度有所改变。同时随着温度的升高,钛箔中白色蠕虫状弥散相 Ti₂Ni 分布得更加均匀。当连接温度达到 875 °C 时,界面处出现了平行于焊缝的大裂纹,各个反应层也变得不再平直,并且焊缝宽度有很大程度上的缩小。从 TiAl/Ti 界面上可以看到,在连接温度为 750 °C, TiAl/Ti 界面处存在两个扩散层分别为 Ti₃Al 层和 Ti(Al)_{ss} 层;当连接温度升高到 800 和 825 °C 时, TiAl/Ti 界面上形成了 3 个扩散层分别为 Ti₃Al 层、Al₃NiTi₂ + Ti₃Al 层、以及 Ti(Al)_{ss} 层;当温度继续升高到 850 °C 时, Ti(Al)_{ss} 层逐渐消失, Al₃NiTi₂ + Ti₃Al 层和 Ti₃Al 层显著长大。分析认为随着温度的升高, TiAl 合金中的铝与钛箔中的钛互扩散更加强烈,使得 Ti(Al)_{ss} 层中铝含量增加,当超过一定的极限后,就会生成 Ti₃Al, 这导致在 TiAl/Ti 一侧界面上 Ti₃Al 层变厚, Ti(Al)_{ss} 逐渐变薄。从 Ti/Ni 界面上可以看到,当温度较低时,界面处存在着一连串的柯肯达尔孔洞,当温度升高时,材料的屈服强度降低,塑性变好,因此在压力下,柯肯达尔孔洞就会闭合。并且随着温度的

升高, TiNi 层得到了明显的长大, Ti₂Ni 层厚度变化较小,而 Ni₃Ti 厚度基本不随温度的变化而改变。

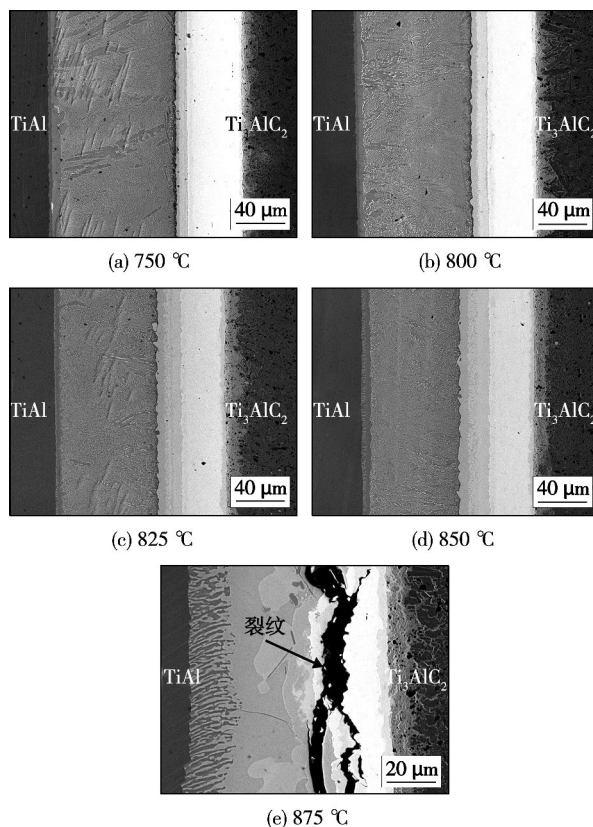


图 6 不同温度下 TiAl/Ti/Ni/Ti₃AlC₂ 接头界面组织形貌
Fig. 6 Interfacial microstructure of TiAl/Ti/Ni/Ti₃AlC₂ joint bonded at different temperature

图 7 显示了试验温度下 5 个试样抗剪强度的平均值与连接温度的关系。从图 5 中可以看到,接头的抗剪强度随着温度的变化呈现出先增大后减小的趋势。当连接温度为 850 °C,保温时间为 60 min,连接压力 30 MPa 时,接头的最高抗剪强度达到 85.2 MPa。当连接温度为 750 °C 时, Ti/Ni 的界面上存在

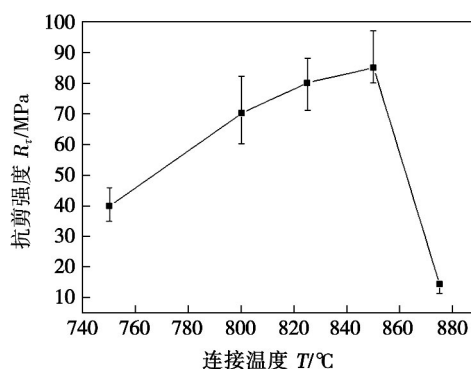


图 7 连接温度对接头抗剪强度的影响

Fig. 7 Effect of bonding temperature on shear strength of joints

着一连串的柯肯达尔孔洞,既降低了焊合率,也容易产生应力集中,因此接头强度较低。随着温度的升高,材料的屈服强度逐渐下降,Ti/Ni 界面上的孔洞闭合,界面的结合更加牢固,强度逐渐提高。但当温度继续升高至 875 °C 时,Ti/Ni 复合中间层剧烈的扩散反应,导致界面处形成了大量 Ti-Al-Ni 三元金属间化合物,且由于焊后冷却速度较快,TiAl 合金与 Ti_3AlC_2 陶瓷之间线膨胀系数差异较大,接头区域产生了大的残余应力致使脆性化合物开裂,导致在钎缝内形成了贯穿性裂纹(图 6e),因此接头抗剪强度急剧下降。

图 8 为在连接温度 850 °C,保温时间为 60 min,连接压力 30 MPa 条件下获得的接头断口形貌。从图 8 中可以看出,断口一小部分位于 I 区(Ni/ Ti_3AlC_2 的界面上),很大一部分位于陶瓷基体上。裂纹首先在 Ni/ Ti_3AlC_2 界面处萌生,接着扩散到陶瓷基体内部,最终断裂在陶瓷上,这是较为理想的断裂模式。为了确定接头断裂位置,对断口 I 区进行选区 XRD 分析,结果如图 9 所示。综合断口形貌与上述分析可知,压剪过程中,裂纹主要沿着 $\text{Ni}_3(\text{Ti,Al})$ 层扩展。

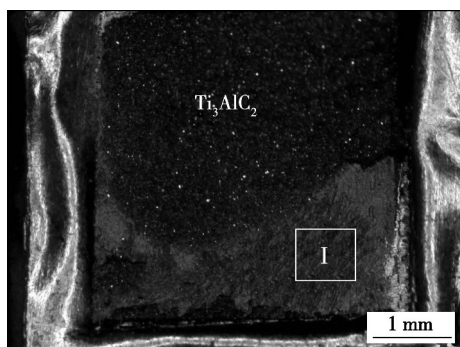


图 8 接头剪切断口的宏观形貌

Fig. 8 Fracture morphology of TiAl/Ti/Ni/ Ti_3AlC_2 joint bonded at 850 °C for 60 min under 30 MPa

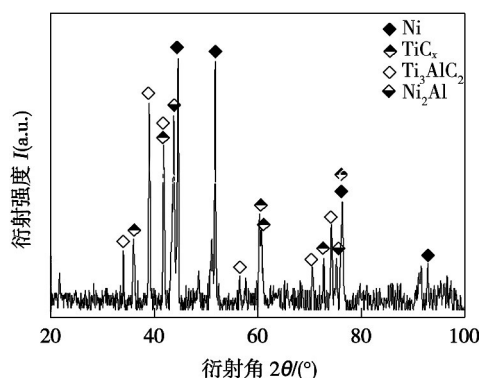


图 9 接头断口 I 区 XRD 结果

Fig. 9 XRD results of area I in fracture surface

3 结 论

(1) 采用 Ti/Ni 复合中间层实现了 TiAl 合金和 Ti_3AlC_2 陶瓷的扩散连接,接头典型界面结构为 $\text{Al}_3\text{NiTi}_2 + \text{Ti}_3\text{Al}/\text{Ti}_3\text{Al}/\alpha\text{-Ti} + \text{Ti}_2\text{Ni}/\text{Ti}_2\text{Ni}/\text{NiTi}/\text{Ni}_3\text{Ti}/\text{Ni}/\text{Ni}_3(\text{Ti,Al})/\text{Ni}_3\text{Al} + \text{TiC}_x + \text{Ti}_3\text{AlC}_2$ 。

(2) 随着连接温度的升高,接头抗剪强度先增大后减小,当连接温度为 850 °C 时,接头抗剪强度最大为 85.2 MPa。

(3) 接头的断裂位置位于 Ni/ Ti_3AlC_2 界面和陶瓷内部基体上。

参考文献:

- [1] Pietzka M A, Schuster J C. Summary of constitutional data on the aluminum-carbon-titanium system[J]. Journal of Phase Equilibria, 1994, 15(4): 392-400.
- [2] 张静平,梅炳初. 三元纳米层状化合物 $\text{M}_{n+1}\text{AX}_n$ 性能和应用[J]. 江苏陶瓷, 2006, 39(4): 21-23.
Zhang Jingping, Mei Bingchu. Performance and application of $\text{M}_{n+1}\text{AX}_n$ compounds[J]. Jiangsu Ceramics, 2006, 39(4): 21-23.
- [3] 刘甲坤,元钧雷,曹健,等. DD3 高温合金与 Ti_3AlC_2 陶瓷的真空钎焊[J]. 焊接学报, 2014, 35(3): 41-44.
Liu Jiakun, Qi Junlei, Cao Jian, et al. Vacuum brazing DD3 superalloy to Ti_3AlC_2 ceramic[J]. Transactions of the China Welding Institution, 2014, 35(3): 41-44.
- [4] 陈秀娟,李建伟. Ti_3AlC_2 陶瓷材料的研究进展[J]. 粉末冶金工业, 2008, 18(4): 40-44.
Chen Xiujuan, Li Jianwei. The research progress of ceramic materials Ti_3AlC_2 [J]. Powder Metallurgy Industry, 2008, 18(4): 40-44.
- [5] Lee S J, Wu S K, Lin R Y. Infrared joining of TiAl intermetallics using Ti-45Cr-45Ni foil-I. the microstructure morphologies of joint interfaces[J]. Acta Materialia, 1998, 46(4): 1283-1295.
- [6] 何鹏,李海新,林铁松,等. TiAl 合金与镍基高温合金的扩散连接[J]. 焊接学报, 2012, 33(1): 17-20.
He Peng, Li Haixin, Lin Tiesong, et al. Diffusion bonding of TiAl to Ni-based superalloy[J]. Transactions of the China Welding Institution, 2012, 33(1): 17-20.
- [7] 曹健,宋晓国,王义峰,等. $\text{Si}_3\text{N}_4/\text{Ni}/\text{TiAl}$ 扩散连接接头界面结构及性能[J]. 焊接学报, 2011, 32(6): 1-4.
Cao Jian, Song Xiaoguo, Wang Yifeng, et al. Interfacial microstructure and properties of $\text{Si}_3\text{N}_4/\text{Ni}/\text{TiAl}$ joint bonded by diffusion bonding[J]. Transactions of the China Welding Institution, 2011, 32(6): 1-4.

作者简介: 宋晓国,男,1983 年出生,博士,讲师。主要从事先进材料和异种材料钎焊及扩散焊方面的科研和教学工作。发表论文 40 余篇。Email: songxg@hitwh.edu.cn

通讯作者: 曹健,男,副教授。Email: cao_jian@hit.edu.cn

MAIN TOPICS ABSTRACTS & KEY WORDS

Development of self-shielded flux cored wire for X100 pipeline steel and performance analysis of welded joints

ZHANG Min , LIU Mingzhi , CHEN Yangyang , LI Jihong (College of Material Science and Engineering , Xi'an University of Technology , Xi'an 710048 , China) . pp 1 - 4

Abstract: The alloy systems of weld metal of X100 pipeline steel were determined with the principle of composition match and structure match. Combined with the principle of weld metal alloying , the types and content of alloy elements which need to transit in the weld can be quantitatively calculated , based on which the flux-cored wire match to X100 pipeline steel was designed and made. The appropriate welding process parameters for welding and the according joint performance were also analyzed. The results showed that the flux-cored wire has excellent mechanical properties with the tensile strength up to 795 MPa , yield strength up to 615 MPa and impact energy value to 47.7J(-40 ℃) . The microstructure of the weld metal consists of lath bainite , granular bainite , and little acicular ferrite , which can match well with base material.

Key words: X100 pipeline steel; flux-cored wire; self-shielded; mechanical properties; alloying

Effects of longitudinal magnetic field on non-consumable gas shielded arc welding

CHEN Shujun¹ , MENG Danyang² , SU Zaiwei² , JIANG Fan¹ , LU Yongsheng¹ (1. College of Mechanical Engineering and Applied Electronics Technology , Beijing University of Technology , Beijing 100124 , China; 2. Tianjin Aerospace Long March Rocket Manufacturing Co. Ltd. , Tianjin 300462 , China) . pp 5 - 8

Abstract: Based on theoretical analysis and experimental method , a set of parallel longitudinal magnetic field generating device is used on the non-consumable gas shielded arc welding process , which includes plasma arc welding and tungsten arc welding. With the use of a high-speed video camera observation the arc shape are measured. Then the arc changes of the two kinds of welding method under the longitudinal magnetic field are compared. The experiment results refer that owing to the specificity of the composition of the plasma arc , the differences between the two kinds of the welding method under the same magnetic field occur. And by means of making analysis of the movement of the particle , the particle motion model is established under the longitudinal magnetic field. It illustrates that because of the difference of the longitudinal velocity of the particles the difference of the motion stage of the charged particles under the longitudinal magnetic field will appear , which explains that why the difference of the arc shape changes exists between the two non-consumable gas shielded arc welding under the same magnetic field.

Key words: longitudinal magnetic field; non-consumable gas shielded arc welding; arc force analysis; particle motion model

Effect of bonding temperature on interfacial microstructure and properties of TiAl/Ti₃AlC₂ joint

SONG Xiaoguo^{1,2} ,

WANG Meirong² , LIN Xingtao¹ , LIU Jiakun¹ , CAO Jian^{1,2} , FENG Jicai^{1,2} (1. State Key Laboratory of Advanced Welding and Joining , Harbin Institute of Technology , Harbin 150001 , China; 2. Shandong Provincial Key Laboratory of Special Welding Technology , Harbin Institute of Technology at Weihai , Weihai 264209 , China) . pp 9 - 12

Abstract: Diffusion bonding of TiAl alloy and Ti₃AlC₂ ceramic was achieved by using Ti/Ni composite interlay. The interfacial microstructure of TiAl/Ti₃AlC₂ joint was analyzed by SEM , EDS and XRD , and was determined as TiAl/Ti₃Al + Al₃NiTi₂/Ti₃Al/α-Ti + Ti₂Ni/Ti₂Ni/TiNi/Ni₃Ti/Ni/Ni₃ (Ti , Al) /Ni₃Al + TiC_x + Ti₃AlC₂/Ti₃AlC₂. As the bonding temperature increased , the thickness of Ti₃Al in TiAl/Ti interface gradually reduced , the Ti₃Al intermetallic layer gradually thickened , and the thickness of TiNi intermetallic layer increased significantly , while the thickness of Ti₂Ni and Ni₃Ti intermetallics layers remained substantially constant. The shear strength of joints first increased and then decreased with increasing the bonding temperature. The maximum shear strength of the joint can reach 85.3 MPa when bonded at 850 ℃ . The joint fracture occurred mainly in Ni/Ti₃AlC₂ interface and Ti₃AlC₂ matrix.

Key words: TiAl alloy; ceramic; diffusion bonding; interfacial microstructure

Study on phase matching control system for pulsed laser-arc hybrid welding based on Labview

SONG Gang , LIU Che , SONG Qiuping , LIU Liming (Key Laboratory of Liaoning Advanced Welding and Joining Technology , School of Materials Science and Engineering , Dalian University of Technology , Dalian 116024 , China) . pp 13 - 16

Abstract: This article introduced a pulsed laser-arc hybrid welding phase matching control system based on Labview. Using NI's PCI6221 data acquisition card , the DAQ system acquired current of AC arc signal , processed the signal and capture the feature points of arc by the computer , thus accurately analyzed the phase of AC arc , and realized a continuous trigger control of pulsed laser on specific phase of AC arc. The locking trigger method was put forward , which eliminated the wrong trigger of laser , realized frequency doubling of pulsed laser and arc and trigger frequency protection of laser. The verifying experiment indicated that the system realized a accurately trigger control of specific phase of arc and the pulsed laser , and also provided the technical support of flexible combination of energy of pulsed laser and AC arc and the research on mechanism of interaction between the two heat resource.

Key words: welding; laser-arc hybrid welding; phase matching; control system

Numerical analysis of three-wire tandem submerged arc welding grade X80 pipeline steel

ZHAO Ming , WANG Haiyan , WAN Fuwei , LUO Detong (College of Mechanical and Electronic Engineering , China University of Petroleum , Qingdao 266580 , China) . pp 17 - 20

Abstract: A model for the thermal process in three-wire